Archives of Civil and Mechanical Engineering (2020) 20:102
https://doi.org/10.1007/s43452-020-00106-1

ORIGINAL ARTICLE

Mechanical properties enhancement of cast Al-8.5Fe-1.3V-1.7Si (FVS0812) alloy by friction stir processing

Z. Nouri[1] · R. Taghiabadi[1] · M. Moazami-Goudarzi[2]

Received: 13 May 2020 / Revised: 3 August 2020 / Accepted: 24 August 2020

Abstract
This study was conducted to investigate the capability of multi-pass friction stir processing (FSP) on microstructure modification and mechanical properties improvement of FVS0812 alloy. FSP was performed at different rotation speeds (1250, 1600, 2000, and 2500 rpm) and traverse speeds (8, 12, and 25 mm/min) for one, two, and four passes. According to the results, applying single-pass FSP at optimized conditions (i.e. 1600 rpm and 12 mm/min) enhanced the tensile strength, fracture strain, and microhardness of the alloy by about 1020, 1050, and 60%, respectively. This improvement can be mainly attributed to the intense breakage and uniform distribution of θ-$Al_{13}Fe_4$ and α-$Al_{12}(Fe,V)_3Si$ intermetallics within the matrix, formation of ultrafine recrystallized grains, and elimination of casting defects. Increasing the number of FSP passes up to four slightly decreased the average size of intermetallic particles, but significantly improved their distribution within the matrix which led to 18 and 200% improvement of tensile strength and fracture strain of one-pass FSPed sample, respectively. The fractography results also revealed that multi-pass FSP has changed the fracture mode of Al-8.5Fe-1.3V-1.7Si alloy from low-energy brittle to a more ductile-dimple fracture.

Keywords Friction stir processing (FSP) · Al-Fe-V-Si · Intermetallic · Mechanical properties

1 Introduction

Due to their high specific strength, excellent castability, good weldability, and high corrosion resistance, commercial Al alloys have been extensively employed in different industrial fields such as automotive, aerospace, and aviation [1]. However, owing to dissolution and/or coarsening of the strengthening precipitates and/or growth of grains, their application is usually limited to the temperatures below 150 °C [2, 3]. Therefore, to increase the service temperature of Al alloys, transition metals such as Fe, Ni, and V are added to their composition. These elements have very low solid-solubility in Al. Therefore, upon solidification, they are severely segregated to the remaining liquid leading to the crystallization of intermetallics rich in transition metals in the microstructure. These precipitates are highly stable at high-temperature services, thereby substantially enhancing the alloy properties up to 450 °C provided that they are finely distributed within the matrix [3]

Therefore, high-temperature Al alloys containing transition metals are often produced by rapid solidification processing (RSP) techniques such as melt spinning [4], spray deposition [5], and gas atomizing [6] which are usually followed by consolidation processes such as hot extrusion, hot pressing, mechanical alloying, and selective laser melting. The high solidification rate of these processes (typically 10^2–10^7 K/s) promotes the formation of ultrafine grains and microstructures, extends solid solution by solute trapping, and inhibits the formation of detrimental compounds such as coarse needle-like θ-$Al_{13}Fe_4$ in the microstructure leading to much better high-temperature properties [7, 8].

However, RSP techniques have some limitations such as high capital cost of equipment and their multi-step nature that impair their widespread application. It has been also shown that, due to the large surface-to-volume ratio of

✉ R. Taghiabadi
taghiabadi@ikiu.ac.ir

Z. Nouri
zibanouri89@yahoo.com

M. Moazami-Goudarzi
moazami@srbiau.ac.ir

[1] Department of Materials Science and Metallurgy, Imam Khomeini International University, Qazvin, Iran

[2] Department of Materials Science, Islamic Azad University, Science and Research Branch, Tehran, Iran

Published online: 02 September 2020

rapidly solidified ribbons/powders, high amounts of oxides are likely to be incorporated into the microstructure of RSPed components. In addition, increasing the temperature in the course of the subsequent processes such as consolidation and extrusion might negatively affect the desired microstructure and the mechanical properties of components [7].

Accordingly, attempts have been made to fabricate Al-Fe-X (X = transition metals) by cost-effective processes such as casting. However, under the low solidification rates of conventional casting processes, the intermetallic compounds are mostly crystallized as large plate-like or irregular-shaped particles that severely deteriorate the mechanical properties, especially the tensile strength and ductility [9]. To overcome this drawback, it is crucial to modify the cast microstructure of Al-Fe-X alloys by appropriate methods such as chemical modification, heat treatment, thermo-mechanical processing, severe plastic deformation, etc. However, a limited number of studies have been conducted so far on the microstructure and mechanical properties of conventionally-cast Al-Fe-X alloys. Sahoo et al. studied the effect of Mg and Ni-Mg modification on the microstructure of conventionally-cast Al-8.3Fe-0.8V-Si alloys [10, 11]. According to their results, adding appropriate amounts of Mg and/or Ni considerably modifies the morphology, size, and distribution of $Al_{13}Fe_4$ intermetallics. They justified this modification by changing the growth morphology of intermetallics through interfacial segregation of Mg and Ni atoms and/or their absorption into the lattice of intermetallics. In another work, they demonstrated the positive impact of Mg and/or Ni-Mg modification on wear resistance and friction behavior of conventionally-cast Al-8.3Fe-0.8Fe-0.9Si alloy [12]. The effect of Ni-Mg modification and subsequent hot rolling/hot extrusion on the ultimate tensile strength (UTS) of Al-Fe-V-Si alloys has been also investigated [13]. The chemically-modified hot-rolled Al-8Fe-1V-1Si alloy had the best properties and its UTS (~ 370 MPa) was higher than that of chemically-modified, hot extruded, and unmodified alloys by 20, 120, and 235%, respectively. Liu et al. [14] investigated the effect of Ce addition on microstructure and mechanical properties of Al-5.5Fe-1.1V-0.6Si alloy produced under near-rapid solidification cooling rate (~ 30 °C/s). They found that adding Ce refines the coarse primary $Al_{13}(Fe,V)_3Si$ intermetallics and improves the alloy mechanical properties where its tensile strength and elongation increased by 76 and 73%, respectively.

FSP [15] is an efficient severe plastic deformation (SPD) technique capable of effectively modifying the microstructure and improving mechanical properties of alloys. In this process, a rotating shouldered tool is plunged into the alloy surface until its shoulder touches the surface. Then, the tool is traversed along the desired direction to encourage microstructural modification/densification through frictional heating and intensive mechanical mixing at the processing zone. FSP effectiveness in enhancing the mechanical properties of brittle alloys and composites has been previously confirmed. Fekri et al. [16] demonstrated that, due to the refinement and changing the morphology/distribution of coarse FeNi-rich intermetallics in the matrix as well as microstructural densification, applying FSP substantially improves the mechanical properties of Al-7Fe-5Ni alloys. In [17], the authors indicated that multi-pass FSP significantly increases tensile strength and ductility of hypereutectic Al-Si alloys. Decreasing the size and changing the morphology of primary silicon particles are the most important factors responsible for the brittle-to-ductile transition. Moharrami et al. [18] showed that FSP can effectively modify the as-cast microstructure of Al-20Mg_2Si composite through refinement and changing the morphology of primary and eutectic Mg_2Si particles and improving their distribution within the matrix. This greatly enhanced the hardness and tribological properties of the composite.

However, to the best of our knowledge, no attempts have been made to modify the as-cast microstructure and improve the mechanical properties of heat-resistant Al-Fe-V-Si alloys by FSP. Therefore, the aim of this study is to investigate the capability of the FSP process, as an efficient, economic, and simple-to-use alternative to the other modification techniques, in improving the mechanical properties of conventionally-cast Al-8.5Fe-1.3V-1.7Si (FVS0812) alloy. This alloy is the most attractive one among RSPed Al-Fe-V-Si alloys owing to its good combination of room and elevated temperature strength and ductility [19].

2 Materials and methods

The experimental Al-8.5Fe-1.3V-1.7Si (wt%) alloy was prepared by melting high purity Al (99.9 wt%), Al-20Fe, Al-30Si, and Al-15V master alloys in an induction furnace (380 V, 37 A, and 10 kHz) under the protection of pure Ar (99.999 wt%). After melting, sufficient time was given to reach a melt with homogenized composition. Thereafter, the melt was degassed by dry C_2Cl_6 (1 wt% of alloy), superheated up to 850 °C, skimmed, and gently stirred by a graphite rod before being poured into a preheated cast-iron mold (250 °C) to obtain slabs with dimensions of 150 × 100 × 10 mm. The average cooling rate of the mold was 4.8 °C/s. The chemical analysis of the alloy is given in Table 1.

The as-cast slabs were subjected to FSP using a plain cylindrical tool made of an AISI H13 tool steel with the hardness of 58 ± 2 HRC, as the most common tool material for the FSP of Al alloys [20, 21]. The geometry and

Table 1 Chemical composition of the base FVS0812 alloy

Fe	Si	V	Other	Al
8.41 ± 0.03	1.73 ± 0.03	1.34 ± 0.02	< 0.1	Rem.

dimension of the tool are shown in Fig. 1a. The FSP process was conducted at different rotation speeds of 1250, 1600, 2000, and 2500 rpm and traverse speeds of 8, 12, and 25 mm/min for one, two, and four passes. These are optimum parameters that lead to the production of samples free of voids, cracks, and other visual major defects. The tool plunge depth was set to 0.3 mm. The FSPed samples were coded as XXXX-XX-nP, where the first and second parts denote the rotation and traverse speeds in rpm and mm/min, respectively, and the third part (after the dash) shows the number of applied passes.

The Vickers hardness of the samples was measured using an HVS-1000A hardness tester under the applied load of 500 g for the dwelling time of 15 s. The average value of six indentations was reported as the final value. The tensile samples were taken from the processed area parallel to the FSP direction (Fig. 1b). The tensile tests were conducted by a Zwick/Roell-Z100 universal testing machine at the crosshead speed of 0.1 mm/min and the average mechanical properties of three tensile tests were reported. The X-ray diffraction analysis (XRD) was performed using Philips X'pert PRO (Cu-Kα radiation) diffractometer with a step size of 0.02 and a step time of 1 s. The samples for metallographic examinations, taken from the processed area normal to the FSPed direction, were prepared by standard metallographic procedures and etched by the Keller's reagent (1 mL HF, 1.5 mL HCl, 2.5 mL HNO_3, and 95 mL distilled water) for 10 s. Microstructural observations were performed by a Tescan-Vega scanning electron microscope (SEM) equipped with an energy-dispersive X-ray spectrometer (EDS) for qualitative chemical analyses. The fractography of the fractured specimens was also performed using the SEM. The porosity content of the samples was measured by the Archimedes' principle as described comprehensively by Taylor et al. [22].

3 Results and discussion

3.1 Microstructural characterization

Figure 2 shows the as-cast microstructure of base (FVS0812) alloy. As seen, the main microconstituents of the base alloy are light gray needle-like and dark gray irregular-shaped intermetallics. According to the EDS analysis results shown in Fig. 3, the chemical composition of needle-like and irregular-shaped particles are well consistent with the analysis of monoclinic θ-$Al_{13}Fe_4$ [10] and body centered cubic α-$Al_{12}(Fe,V)_3Si$ [23] compounds mentioned elsewhere. The extensive formation of micropores is also evident in the microstructure. As it is evident from the micrographs, the majority of micropores have been formed as a result of shrinkage due to blocking the liquid feeding paths by the primary $Al_{13}Fe_4$ needles. However, as demonstrated by Anyalebechi [24], the rejection of H-atoms into the remaining liquid ahead of solidification front is an essential mechanism encouraging the formation of mixed (gas and shrinkage) microporosities, especially in the presence of elements such as Fe which reduces the hydrogen solubility in molten Al.

Figure 4a depicts the SEM microstructure of the boundary between the stir zone (SZ) and unaffected base metal (BM) in FVS0812 sample. As seen, due to the synergic effect of frictional heating and severe plastic strains applied during FSP tool stirring [15], both α and θ intermetallics in the SZ have been extremely broken down and evenly distributed within the matrix. The enlarged micrographs illustrating the SZ microstructure of 1600-12-1P, 1250-12-1P, and 2500-12-1P samples are shown in Fig. 4b–d, respectively. As seen, in agreement with the image analysis results (Table 2), increasing the rotation speed has refined the intermetallic particles, trimmed off their sharp edges, and improved their distribution within the SZ. It is also evident from the micrographs that the existing micropores have been effectively

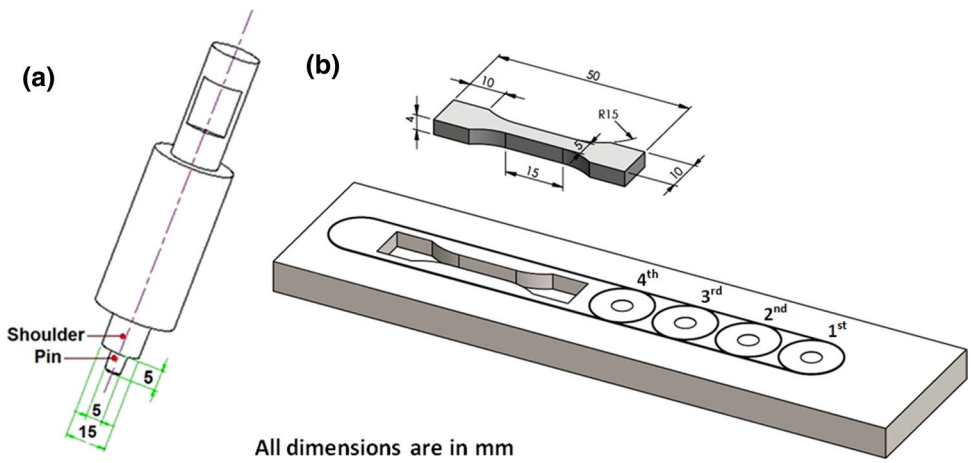

Fig. 1 Geometry and dimensions of **a** FSP tool and **b** tensile test sample and sampling location on four-pass FSPed sample

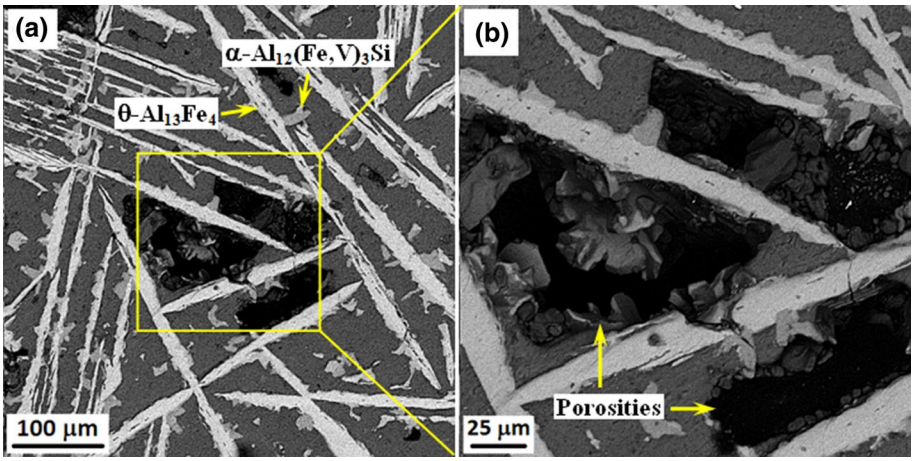

Fig. 2 **a** As-cast microstructure of the base FVS0812 alloy and **b** enlarged view of the boxed area in micrograph 2a

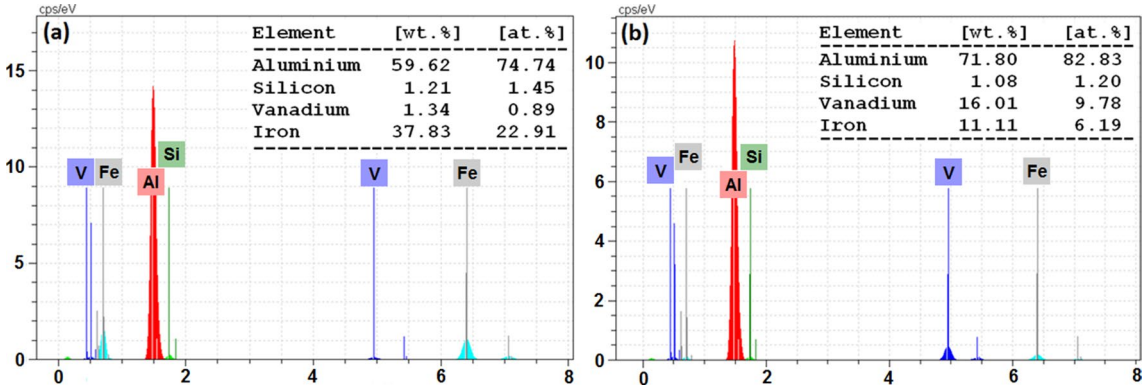

Fig. 3 EDS spectrum of **a** θ-$Al_{13}Fe_4$ and **b** α-$Al_{12}(Fe,V)_3Si$ shown in Fig. 2a

refined in the SZ. According to the Archimedes' test, the volume fraction of micropores has been reduced from about 3% in as-cast Base sample to about 0.55% in 1600-1P (Table 2). This can be attributed to the effective forging of micropores as a result of intense plastic flow of the softened material in the SZ.

FSP also effectively refines the SZ grains. Figure 5a compares the XRD patterns of the base and 1600-12-1P samples. Figure 5b also illustrates the locally-enlarged view of XRD profile at $2\varphi = 40°–50°$. As seen, FSP has shifted the peaks corresponding to the α-Al matrix to the lower angles and broadened the full width at half maximum (FWHM). According to [25] the former can be attributed to the residual stress developed in the course of FSP while based on [26] the latter can be related to the lower size of the grains. Williamson-Hall equation (Eq. 1) can be successfully used to determine the crystallite size [27]:

$$\beta \cos \varphi = \frac{0.9\lambda}{t} + \left(\frac{\Delta d}{d}\right) 4 \sin \varphi, \tag{1}$$

where λ is the X-ray wavelength, β is the line broadening at FWHM after subtracting the instrumental line broadening (in radians), φ is the Bragg angle (in degrees), $\left(\frac{\Delta d}{d}\right)$ is the strain, and t is the crystallite size. Using this approach the average size of crystallite grains in Base and 1600-12-1P samples, estimated from the y-intercept of the graph plotted between $\beta\cos\varphi$ and $4\sin\varphi$ (Fig. 5c), are about 35 and 26 nm, respectively.

Considering the high stacking fault energy of Al and its alloy, the formation of fine equiaxed grains in the SZ of FSPed samples can be attributed to the dynamic recrystallization due to the synergistic effect of severe plastic deformation and heat generation [28]. Figure 5d shows an infrared thermographic image, taken by an AVIO infrared camera, showing the surface temperature of 1600-8-1P sample during its FSP. As seen, due to the frictional heating, severe plastic deformation, and viscous dissipation, the surface temperature of the sample has increased to about 560 °C which seems to be an appropriate value for dynamic recrystallization [29].

The FSP effectiveness in grain refinement has been previously reported elsewhere. According to Ma [15], the refinement of grains is generally due to the occurrence

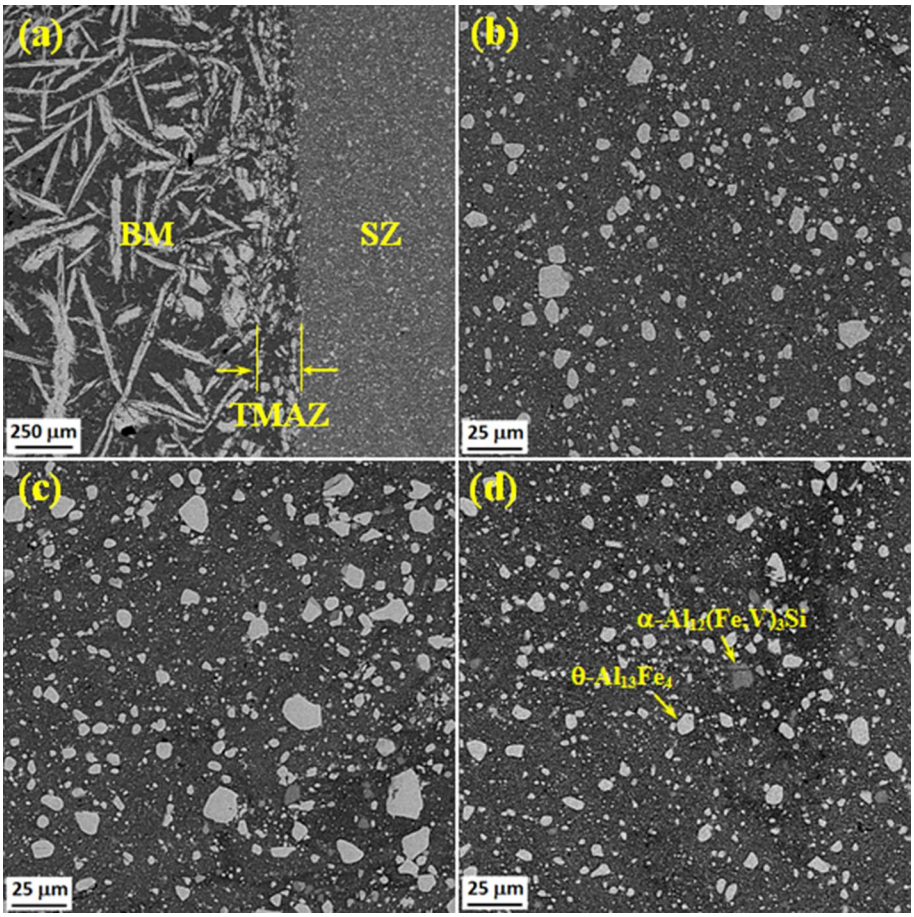

Fig. 4 SEM micrographs showing the microstructure of **a** the boundary between the SZ and BM in 1600-12-1P sample, **b** SZ of 1600-12-1P, **c** SZ of 1250-12-1P, and **d** SZ of 2500-12-1P samples

Table 2 Image analysis results of the base and selected FSPed samples

	Fe-rich intermetallics				Porosities
	Average size, µm		Average aspect ratio		vol%
	Needle-like	Polyhedral	Needle-like	Polyhedral	
Base	275.1 ± 27.4	31.1 ± 9.2	34.23	2.1	3.04
1250-12-1P	–	13.1 ± 4.5	1.5		0.61
2500-12-1P	–	5.5 ± 2.3	1.3		0.52
1600-12-1P	–	8.5 ± 4.3	1.4		0.54
1600-12-2P	–	7.0 ± 4.0	1.2		0.52
1600-12-4P	–	4.4 ± 2.1	1.2		0.47

of dynamic recrystallization. Moharrami et al. [30] also showed that multi-pass FSP can significantly refine the as-cast microstructure of Al-25Mg_2Si composite. Based on their EBSD investigations, a direct relationship was found between FSP passes and the density of grain boundaries. Su et al. also indicated that the combined effect of FSP and rapid cooling results in formation of nano-sized grains in the microstructure of 7075 Al alloy. They attributed this to the occurrence of discontinuous dynamic recrystallization [31].

3.2 Mechanical properties

The effect of FSP on the tensile properties and hardness of FVS0812 alloy is shown in Figs. 6 and 7, respectively. As seen, in the as-cast condition, the alloy exhibits very poor mechanical properties. Considering Fig. 2, this can be attributed to the presence of huge amounts of Fe-rich intermetallics (especially the coarse needle-like θ-$Al_{13}Fe_4$) and intermetallic-related defects in the microstructure. The negative impact of the needle-like Fe-rich intermetallics such as

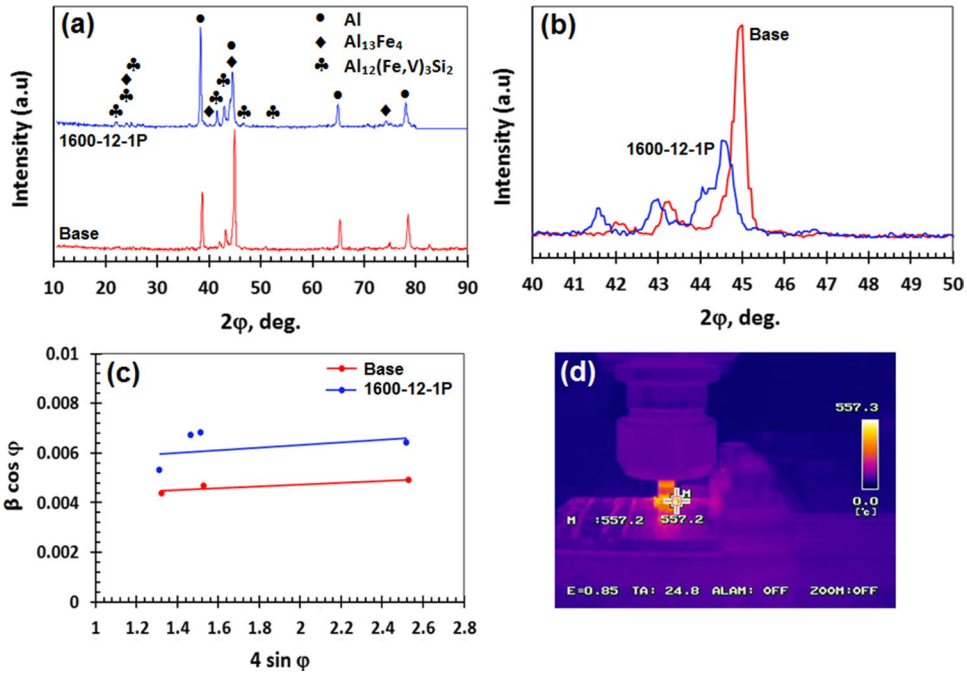

Figure 5 **a** XRD patterns of the base and 1600-12-1P samples, **b** locally-enlarged view of XRD profile at $2\theta = 54°–66°$, **c** Williamson-Hall plots of the base and 1600-12-1P sample, and **d** typical infrared thermography image showing the maximum surface temperature during FSP of 1600-8-1P sample

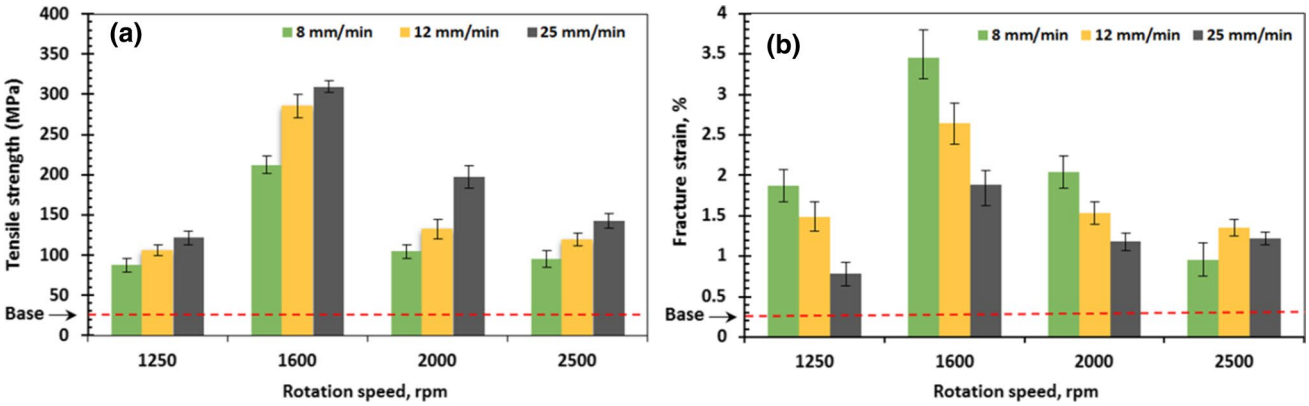

Fig. 6 Effect of FSP parameters on **a** tensile strength and **b** fracture strain of FVS0812 alloy

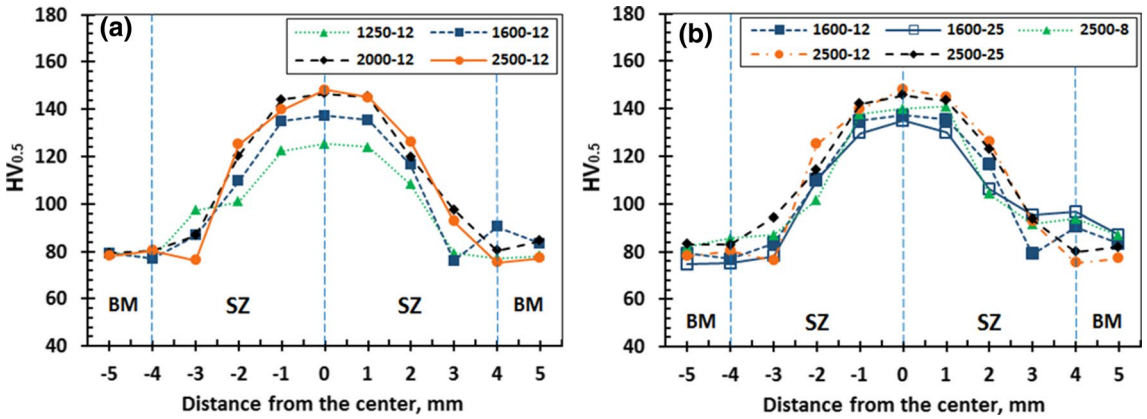

Fig. 7 Effect of **a** rotation speed and **b** traverse speed on hardness profiles of FVS0812 alloy at the mid-thickness of its SZ perpendicular to the FSP direction

θ-$Al_{13}Fe_4$ on mechanical properties of cast Al-based alloys has been extensively studied [32]. These needles, due to their high aspect ratio (Table 2), effectively arrest the motion of dislocations serving as potential stress concentrators within the matrix. However, according to [33], due to the brittle nature arising from their complex crystal structure, they are quite susceptible to microcracking. Moreover, due to their weak smooth-type interfaces stems from their high melting entropy [34], they are prone to detachment from their surrounding matrix. Vorren et al. [35] showed that the detached particles act as two-dimensional defects deteriorating the tensile properties.

In addition to the above, the presence of needle-like intermetallics can greatly increase the volume fraction of micropores in the microstructure (Fig. 2 and Table 2). The gas/shrinkage micropores are detrimental defects that impair the mechanical properties. This is because they decrease the effective load-bearing area serving as stress-concentration points in the castings facilitating the initiation of microcracks. The fracture surface of the base sample is shown in Fig. 8. The presence of fractured θ-$Al_{13}Fe_4$ and α-$Al_{12}(Fe,V)_3Si$ particles (with the EDS analysis shown in Fig. 9) as well as a large shrinkage micropore next to needle-like intermetallics imply their critical role in low-energy brittle fracture of Base sample.

Regardless of the processing parameters, applying FSP substantially improves the tensile properties (Fig. 6). As seen, the highest tensile properties belong to 1600-12-1P sample, where compared to the base sample, its tensile strength and fracture strain have increased by 1020 and 1050%, respectively. However, despite the substantial improvement of tensile properties of FSPed samples, the net value of the fracture strains is low. The variation of hardness across the SZ perpendicular to the FSP direction for the samples FSPed at different processing parameters is also shown in Fig. 7. As seen, FSP has substantially improved the hardness. However, despite the tensile properties, the highest hardness belongs to 2500-12-1P where its peak hardness is 130% higher than the average hardness of its unaffected BM region.

Considering the multilateral effect of FSP on as-cast microstructure/macrostructure of FVS0812 sample, the improved mechanical properties of FSPed samples can be mainly justified by the refinement and uniform distribution

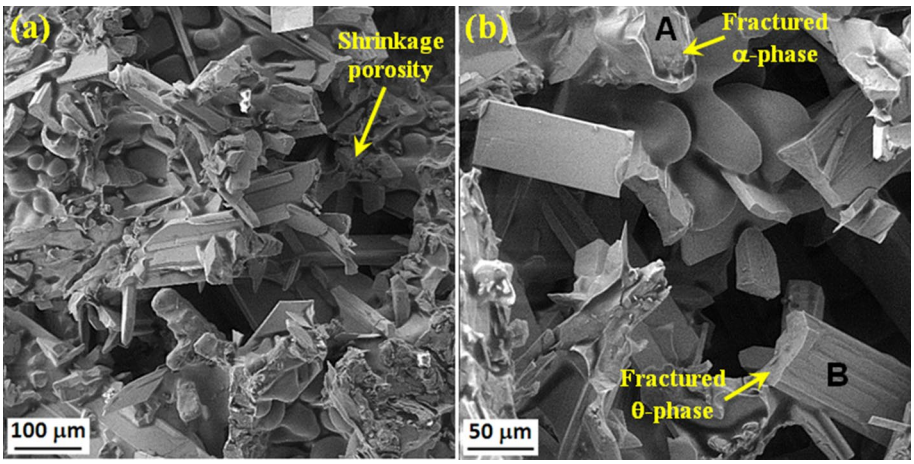

Fig. 8 SEM microfractographs showing the fracture surface of FVS0812 alloy a low magnification and **b** high magnification

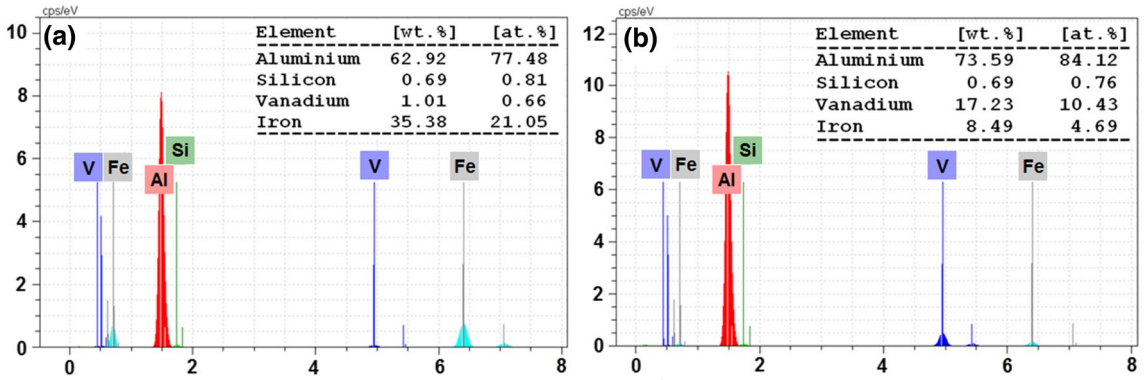

Fig. 9 EDS analysis of the marked points in microfractographs 8b, **a** point A, **b** point B

of their intermetallic compounds, refinement of their grains, and the lower size and volume fraction of micropores in their microstructures. According to Fig. 4 and image analysis results (Table 2), applying the first pass of FSP significantly refines the intermetallic particles and disperses them uniformly within the matrix. Decreasing the aspect ratio and increasing the particles number per unit area substantially lower the level of stress imposed on individual particles, thereby increases their resistance to breaking and/or detachment from the matrix giving rise to a better ductility [36]. The refined particles can also effectively enhance the strength by Orowan mechanism [37] provided that their size becomes small enough that can effectively impede the dislocation motion. Moreover, Sharma et al. [38] and Liu et al. [39] showed that the thermo-mechanical effect of FSP can significantly improve the interfacial bonding strength of second-phases, thereby enhancing their load transfer efficiency, leading to a better mechanical strength and ductility.

Furthermore, the formation of fine dynamically-recrystallized grains (Fig. 5) which increase the density of grain boundaries is an important factor improving the mechanical properties of FSPed samples through grain boundary strengthening mechanism as already demonstrated by Shaeri et al. [40]. Meanwhile, as stated in [41], the large number of dislocations exist in or along sub-grain boundaries of recrystallized grains in the SZ. These dislocations can significantly contribute to improving the hardness/strength through interacting with each other or grain boundaries [42].

The fracture surface of 1600-12-1P sample is shown in Fig. 10. As seen, compared to the fracture surface of the base sample (Fig. 8) and in agreement with the tensile properties (Fig. 6), the average size of intermetallic particles has considerably decreased and the dimples, a typical feature of a ductile fracture, are observed on the surface. As expected, large intermetallics have been extensively fractured and/or debonded from the matrix (Fig. 10b). This can be explained by the development of high stress-concentrations on these particles mediated by their inconsistent plastic deformation with respect to that of surrounding Al matrix. The fracture and/or debonding of particles can be considered as an important factor responsible for the relatively low fracture strain of 1600-12-1P sample.

Despite the effective refinement of brittle intermetallic compounds and promotion of more homogeneous microstructure (Fig. 4 and Table 2) increasing the rotation speed to 2000 and 2500 rpm adversely affects the tensile properties (Fig. 6). For instance, the tensile strength and fracture strain of 2500-12-1P sample are lower than those of 1600-12-1P by about 50 and 60%, respectively. This can be justified by the growth of grains and/or formation of defects at the higher rotation speeds where due to friction, plastic deformation, and viscous dissipation, considerable amounts of heat is generated within the SZ [43]. Increasing the temperature, on one hand, promotes the growth of SZ grains and, on the other hand, encourages the formation of process-related defects mediated by turbulent flow of material [44]. However, given that the peak hardness of 2500-12-1P sample is higher than that of 1600-12-1P alloy (Fig. 7a) it seems that defect formation is the dominant factor responsible for inferior tensile properties.

The effect of two- and four-pass FSP under the optimized parameters (1600 rpm and 12 mm/min) on the SZ microstructure of FVS0812 alloy is shown in Fig. 11. Moreover, the histogram graphs showing the particles size distribution in 1600-12-1P, 1600-12-2P, and 1600-12-4P samples are shown in Fig. 12. As seen, compared to the microstructure of 1600-12-1P sample (Fig. 4a, b) and in accordance with the image analysis results (Table 2), the average size of fractured intermetallics in multi-pass FSPed samples has relatively decreased so that the amount of particles with the average size of less than 5 µm has considerably increased (Fig. 12). Increasing the number of FSP passes has also substantially improved the distribution of particles.

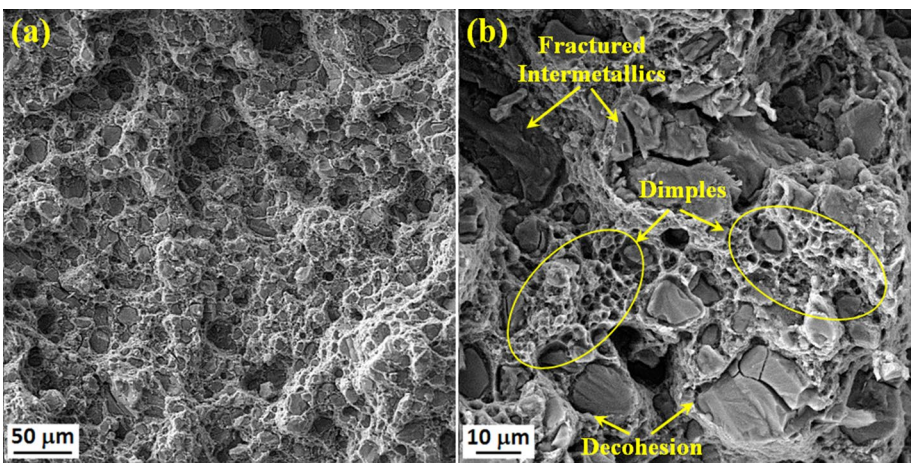

Fig. 10 SEM microfractographs showing the fracture surface of 1600-12-1P sample **a** low magnification and **b** high magnification

These microstructural changes slightly enhance the tensile strength and hardness of the alloy, but substantially improve the fracture strain (Fig. 13). For instance, while the tensile strength and hardness of 1600-12-4P sample have improved by 18 and 23%, respectively, compared to those of 1600-12-1P sample, its fracture strain

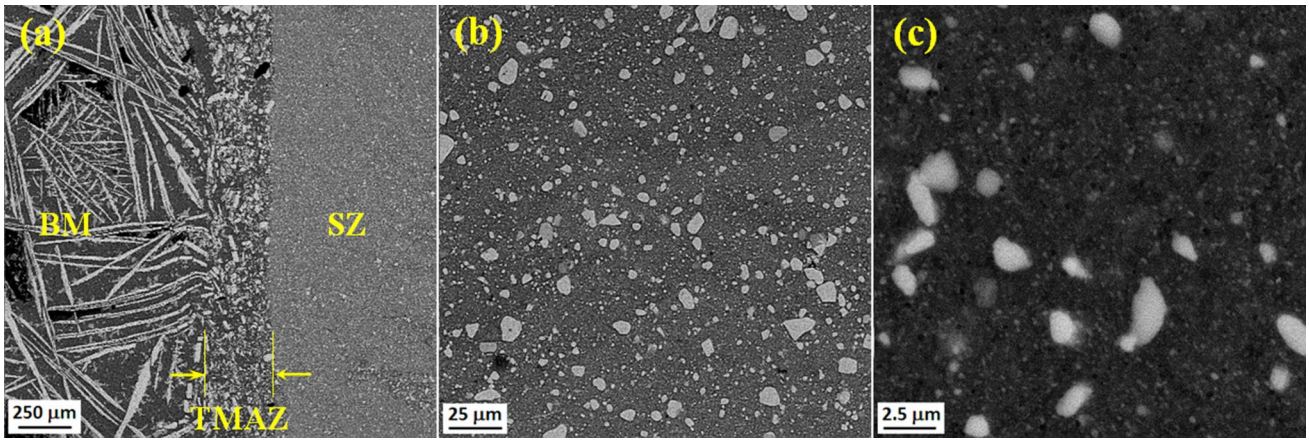

Fig. 11 SEM micrographs showing the microstructure of **a** the boundary between the SZ and BM in 1600-12-4P sample, **b**, **c** SZ microstructure at higher magnifications

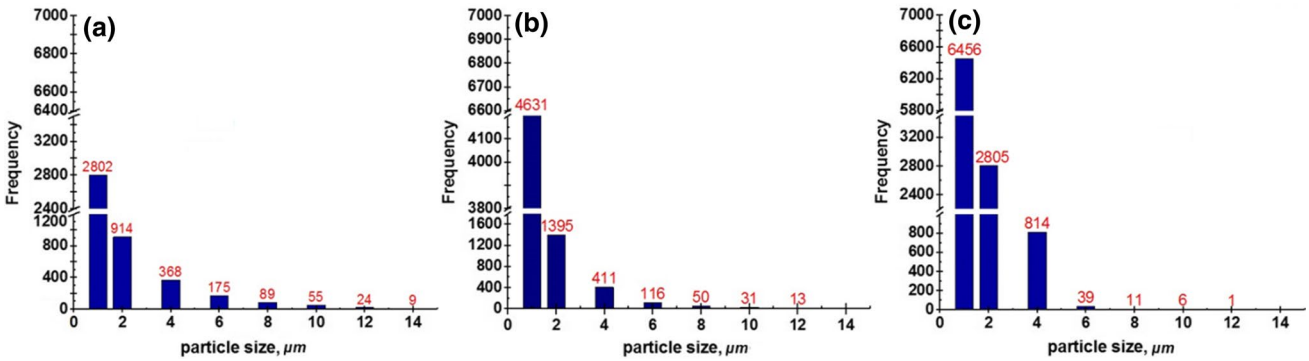

Fig. 12 Histograms showing the distribution of intermetallic particles size in **a** 1600-12-1P, **b** 1600-12-2P, and **c** 1600-12-4P samples

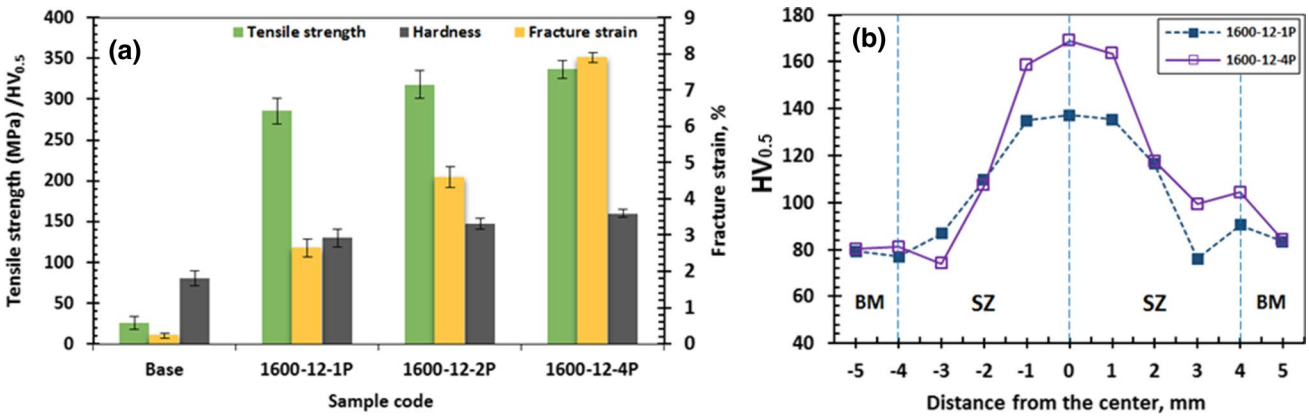

Fig. 13 Effect of multi-pass FSP on **a** tensile strength, hardness, and fracture strain of FVS0812 alloy and **b** hardness profiles at the mid-thickness of SZ perpendicular to the FSP direction

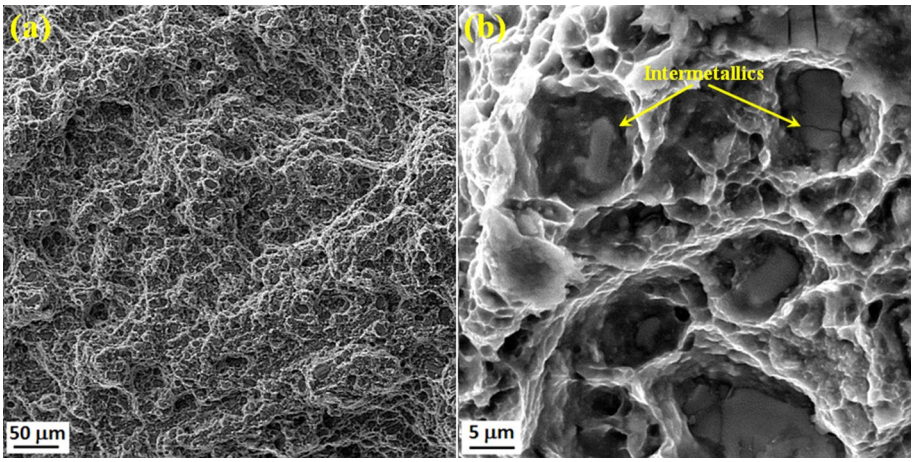

Fig. 14 SEM microfractographs showing the fracture surface of 1600-12-4P sample **a** low magnification and **b** high magnification

has improved by 200%. The relative size reduction of brittle intermetallics, increased fraction of ultrafine particles capable of providing Orowan strengthening, improved bonding strength of the particles/matrix, substantial improvement of particles distribution, and considerable reduction of casting defects can be considered as the most important factors enhancing the mechanical properties of multi-pass processed samples.

The SEM microfractographs showing the fracture surface of 1600-12-4P sample are shown in Fig. 14. As seen, compared to the fracture surface of 1600-12-1P sample (Fig. 10), applying four-pass FSP has extended the dimpled character of fracture surface justifying the improved ductility of sample. The existence of intermetallics at the bottom of dimples (Fig. 14b) also indicates their critical role in the fracture of sample through encouraging the initiation and growth of microvoids and their coalescence into microcrack [42].

The average room-temperature tensile properties of FVS0812 alloy produced by different methods are given in Table 3. For comparison, the average tensile properties of 1600-12-4P sample are also included. As seen, the average tensile strength of 1600-12-4P sample is comparable to or even better than that of the samples fabricated by mechanical alloying followed by extrusion, spray deposition followed by wedge pressing, atomized melt deposition, and atomized melt deposition followed by hot isostatic pressing and extrusion. However, the average elongation of 1600-12-4P sample is about 8% which is among the lowest values presented in the Table 3. This is likely due to the lower effectiveness of FSP in developing sufficiently-refined microstructures comprising of sub-micron grains and appropriate precipitates such as α-$Al_{12}(Fe,V)_3Si$ particles with suitable size capable of effective blockage of dislocation motion.

4 Conclusion

The capability of multi-pass FSP on the microstructure modification and mechanical properties enhancement of conventionally-cast Al-8.5Fe-1.3V-1.7Si (FVS0812) alloy was investigated. Following conclusions can be drawn:

1- Multi-pass FSP resulted in substantial refinement, homogenization, and densification of as-cast microstructure of FVS0812 alloy. The average size of θ-$Al_{13}Fe_4$ platelets has decreased from 275 µm in as-cast alloy to less than about 5 µm in four-pass FSPed sample. The volume fraction of micropores has also reduced from about 3% in as-cast sample to less than 0.5% in four-pass FSPed sample.
2- Applying the first pass of FSP enhanced the tensile strength, fracture strain, and hardness of the alloy by about 1020, 1050, and 60%, respectively. This improvement can be mainly attributed to the intense breakage and uniform distribution of θ-$Al_{13}Fe_4$ and α-$Al_{12}(Fe,V)_3Si$ intermetallics within the matrix, formation of ultrafine recrystallized grains, and elimination of casting defects.
3- Increasing the number of FSP passes up to four slightly decreased the average size of intermetallic particles, but significantly improved their distribution within the matrix which led to 18 and 200% improvement of tensile strength and fracture strain of one-pass FSPed sample, respectively.
4- The tensile strength of four-pass FSPed sample was comparable to or even better than that of samples produced by the common fabrication methods. However, its average fracture strain was lower than that obtained by the common fabrication routes.

Table 3 Comparison of room-temperature tensile properties of 1600-12-4P sample with those of Al-7.8Fe-1.3V-1.8Si samples fabricated by other processes

alloy	Fabrication/processing method	Tensile properties		References
		UTS, MPa	Elongation, %	
Al-7.8Fe-1.3V-1.8Si	MA[a]/EX[b]	281.0	15.0	[45]
Al-8.5Fe-1.3V-1.7Si	EBM[c]	438.0	12.0	[46]
Al-8.5Fe-1.3V-1.7Si	PFC[d]/EX	448	9.1	[47]
Al-8.5Fe-1.3V-1.7Si	SD[e]/EX (350 °C)	435.0	7.0	[48]
	SD/EX (450 °C)	395.0	7.5	
Al-8.5Fe-1.2V-1.7Si	SD/EX	360.5	9.7	[5]
Al-8.0Fe-1.0V-2.0Si	UGA[f]/EX	420	9.2	[49]
Al-8.5Fe-1.3V-1.7Si	SD/Wedge pressing	290	9.0	[50]
Al-8.5Fe-1.2V-1.7Si	ADM[g]	281	9.5	[51]
	ADM/HIP[h]/EX	313	18	
Al-8.4Fe-1.3V-1.7Si	CC[i]/Multi-pass FSP	336.9	7.9	Current study

[a]Mechanical alloying
[b]Extrusion
[c]Electron beam melting
[d]Planar flow casting
[e]Spray deposition
[f]Ultrasonic gas atomization
[g]Atomized melt deposition
[h]Hot isostatic pressing
[i]Conventional casting

Compliance with ethical standards

Conflict of interest The authors had no funding sources or conflict of interest to report.

References

1. Kaufman JG. Fire resistance of aluminum and aluminum alloys: measuring the effects of fire exposure & on the properties of aluminum alloys. First printing, Chapter 1. Materials Park: ASM International; 2016.
2. Rakhmonov J, Timelli G, Bonollo F. The effect of transition elements on high-temperature mechanical properties of Al-Si foundry alloys—a review. Adv Eng Mater. 2016;18:1096–105.
3. Stevam R, Neto RML, Camargo PA, Filho FA. Al-Fe-X-Si (X=V or Nb) alloy powders prepared by high energy milling in an attritor mill. J Metastable Nanocryst Mater. 2004;20–21:207–12.
4. Yaneva S, Petrov K, Petrov R, Stoichev N, Avdeev G, Kuziak R. Influence of silicon content on phase development in Al–Fe–V–Si alloys. Mater Sci Eng A. 2009;515(1–2):59–655.
5. Tang Y, Tan D, Li W, Pan Z, Liu L, Hu W. Preparation of Al–Fe–V–Si alloy by spray co-deposition with added its over-sprayed powders. J Alloys Compd. 2007;439(1–2):103–8.
6. Zheng L, Liu Y, Sun S, Zhang H. Selective laser melting of Al–8.5Fe–1.3V–1.7Si alloy: investigation on the resultant microstructure and hardness. Chin J Aeronaut. 2015;28(2):564–9.
7. Marshall R. Characterization of novel microstructure in Al-Fe-V-Si and Al-Fe-V-Si-Y alloys processed at intermediate cooling rates, Ph.D. Thesis, Faculty and the boards of Trustees of the Colorado school of mines; 2015.
8. Ozyurda HA. Spray rolling of rapidly-solidified Al-Fe-V-Si alloy, Ph.D. Thesis, Middle East Technical University; 2006.
9. Arhami M, Sarioglu F, Kalkanli A, Hashemipour M. Microstructural characterization of squeeze-cast Al–8Fe–1.4V–8Si. Mater Sci Eng A. 2008;485:218–23.
10. Sahoo KL, Das SK, Murty BS. Formation of novel microstructures in conventionally cast Al–Fe–V–Si alloys. Mater Sci Eng A. 2003;355(1–2):193–200.
11. Sahoo KL, Sivaramakrishnan CS, Chakrabarti AK. Modification of cast structure in Al–8.3Fe–0.8V–0.9Si alloy by magnesium treatment. Mater Sci Technol. 2000;16(2):227–30.
12. Sahoo K, Krishnan CS, Chakrabarti A. Studies on wear characteristics of Al–Fe–V–Si alloys. Wear. 2000;239(2):211–8.
13. Sahoo KL, Pathak BN. Solidification behaviour, microstructure and mechanical properties of high Fe-containing Al–Si–V alloys. J Mater Proc Technol. 2009;209(2):798–804.
14. Liu Y-L, Luo L, Shun M-Z, Zhang L, Zhao Y-H, Wu B-L. Microstructure and mechanical properties of Al–5.5Fe–1.1V–0.6Si alloy solidified under near-rapid cooling and with Ce addition. Rare Met. 2016;37(12):1070–5.
15. Ma ZY. Friction stir processing technology: a review. Metall Mater Trans. 2008;39A:642–58.
16. Fekri Soustani M, Taghiabadi R, Jafarzadegan M, Shahriyari F, Rahmani A. Improving the tribological properties of Al-7Fe-5Ni alloys via friction stir processing. J Tribol. 2019;141(12):1–19.
17. Rao AG, Deshmukh VP, Prabhu N, Kashyap BP. Enhancing the machinability of hypereutectic Al-30Si alloy by friction stir processing. J Manuf Proc. 2016;23:130–4.

18. Moharrami A, Razaghian A, Emamy M, Taghiabadi R. Effect of tool pin profile on the microstructure and tribological properties of friction stir processed Al-20 wt% Mg_2Si composite. J Tribol. 2019;141(12):122202.
19. Sun S, Zheng L, Liu Y, Liu J, Zhang H. Characterization of Al–Fe–V–Si heat-resistant aluminum alloy components fabricated by selective laser melting. J Mater Res. 2015;30(10):1661–9.
20. Rai R, De A, Bhadeshia HKDH, DebRoy T. Review: friction stir welding tools. Sci Technol Weld Join. 2011;16(4):325–42.
21. Zhang YN, Cao X, Larose S, Wanjara P. Review of tools for friction stir welding and processing. Can Metall Q. 2012;51(3):250–61.
22. Taylor RP, McClain ST, Berry JT. Uncertainty analysis of metal-casting porosity measurements using Archimedes' principle. Int J Cast Metals Res. 1999;11(4):247–57.
23. Zou Q, Zhao M, Yin F, Li Z, Liu Y. Phase equilibria in the Al-rich corner of the Al-Fe-Si-V quaternary system at 620 °C. J Phase Equilib Diffus. 2017;36(3):274–82.
24. Anyalebechi PN. Analysis of the effects of alloying elements on hydrogen solubility in liquid aluminum alloys. Scrip Metall Mater. 1995;33(8):1209–16.
25. Węglowski MS, Sedek P, Hamilton C. Experimental analysis of residual stress in friction stir processed cast AlSi9Mg aluminium alloy. Key Eng Mater. 2016;682:18–23.
26. Shahriyari F, Taghiabadi R, Razaghian A, Mahmoudi M. Effect of friction hardening on the surface mechanical properties and tribological behavior of biocompatible Ti-6Al-4V alloy. J Manuf Proc. 2018;31:776–86.
27. Hyett G, Green M, Parkin IP. X-ray diffraction area mapping of preferred orientation and phase change in TiO_2 thin films deposited by chemical vapor deposition. J Am Chem Soc. 2006;128(37):12147–55.
28. Su J-Q, Nelson TW, Sterling CJ. Grain refinement of aluminum alloys by friction stir processing. Philos Mag. 2006;86(1):1–24.
29. Totten GE, Scott MD. Handbook of aluminum: alloy production and materials manufacturing, vol. 2. New York: Marcel Dekker Inc.; 2003.
30. Moharrami A, Razaghian A, Paidar M, Šlapáková M, Ojo OO, Taghiabadi R. Enhancing the mechanical and tribological properties of Mg_2Si-rich aluminum alloys by multi-pass friction stir processing. Mater Chem Phys. 2020;250:123066.
31. Su JQ, Nelson TW, Sterling CJ. Development of ultrafine grained microstructure and low temperature (0.48 Tm) superplasticity in friction stir processed Al–Mg–Zr. Mater Res. 2003;18:1757–60.
32. Mbuya TO, Odera BO, Ng'ang'a SP. Influence of iron on castability and properties of aluminium silicon alloys: literature review. Int J Cast Metals Res. 2016;16(5):451–65.
33. Armbrüster M, Schlögl R, Grin Y. Intermetallic compounds in heterogeneous catalysis-a quickly developing field. Sci Technol Adv Mater. 2014;15(3):34803.
34. Herlach DM, Simons D, Pichon PY. Crystal growth kinetics in undercooled melts of pure Ge, Si and Ge–Si alloys. Philos Trans R Soc A Math Phys Eng Sci. 2018;376(2113):20170205.
35. Vorren O, Evensen JE, Pedersen TB. Microstructure and mechanical properties of AlSi (Mg) casting alloy. AFS Trans. 1984;92:459–66.
36. Hannard F, Castin S, Maire E, Mokso R, Pardoen T, Simar A. Ductilization of aluminium alloy 6056 by friction stir processing. Acta Mater. 2017;130:121–36.
37. Zhang Z, Chen DL. Contribution of Orowan strengthening effect in particulate-reinforced metal matrix nanocomposites. Mate Sci Eng A. 2008;483–484:148–52.
38. Sharma V, Prakash U, Kumar BVM. Surface composites by friction stir processing: a review. J Mater Proc Technol. 2015;224:117–34.
39. Liu L, Bao R, Yi J, Fang D. Fabrication of CNT/Cu composites with enhanced strength and ductility by SP combined with optimized SPS method. J Alloys Compd. 2018;747:91–9.
40. Shaeri MH, Shaeri M, Salehi MT, Seyyedein SH, Djavanroodi F, Abutalebi MR. Effect of ECAP temperature on microstructure and mechanical properties of Al-Zn-Mg-Cu alloy. Prog Nat Sci Mater Int. 2015;25:159–68.
41. Huang KT, Lui TS, Chen LH. Effect of dynamically recrystallized grain size on the tensile properties and vibration fracture resistance of friction stirred 5052 alloy. Mater Trans. 2006;47:2405–12.
42. Yuvaraj N, Aravindan S. Fabrication of Al5083/B4C surface composite by friction stir processing and its tribological characterization. J Mater Res Technol. 2015;4(4):398–410.
43. Shibayanagi T, Gerlich AP, Kashihara K, North TH. Texture in single-crystal aluminum friction spot welds. Metall Mater Trans A. 2009;40A:920.
44. Taghiabadi R, Aria N. Statistical strength analysis of dissimilar AA2024-T6 and AA6061-T6 friction stir welded joints. J Mater Eng Perform. 2019;28:1822–32.
45. Xiao BL, Fan J, Zhou L, Shi L. Microstructure and mechanical properties of Al-Fe-V-Si alloy and composites. J Ceram Proc Res. 2006;7(2):164–6.
46. Sun S, Zheng L, Peng H, Zhang H. Microstructure and mechanical properties of Al-Fe-V-Si aluminum alloy produced by electron beam melting. Mater Sci Eng A. 2016;659:207–14.
47. Liebermann HH. Rapidly solidified alloys: processes, structures, properties, applications. New York: Marcel Dekker Inc.; 1993.
48. Zhang R, Wu B. Effect of TiC particles on microstructure and properties of Al-Fe-V-Si alloy. App Mech Mater. 2014;543–547:3725–8.
49. Prakash U, Raghu T, Gokhale A, Kamat S. Microstructure and mechanical properties of RSP/M Al-Fe-V-Si and Al-Fe-Ce alloys. J Mater Sci. 1999;34:5061–5.
50. Chen ZH, Chen ZG, Yan HG, Chen D, He YQ, Chen G. Novel method for densification of porous spray deposited Al–Fe–V–Si alloy tube performs. Mater Sci Technol. 2009;25(1):111–6.
51. Hariprasad S, Sastry SML, Jerina KL, Lederich RJ. Microstructures and mechanical properties of dispersion-strengthened high-temperature Al-8.5Fe-1.2V-1.7Si alloys produced by atomized melt deposition process. Metall Trans A. 1993;24:865–73.